Available online at www.sciencedirect.com
ScienceDirect
J. of Supercritical Fluids 44 (2008) 466–474
THE JOURNAL OF Supercritical Fluids
www.elsevier.com/locate/supflu

Deposition kinetics and narrow-gap-filling in Cu thin film growth from supercritical carbon dioxide fluids

Eiichi Kondoh *, Junpei Fukuda [1]

Interdisciplinary Graduate School of Medicine and Engineering, University of Yamanashi, 4-3-11 Takeda, Kofu 400-8511, Japan

Received 9 March 2007; received in revised form 11 December 2007; accepted 17 December 2007

Abstract

We have developed a flow-type reaction system that enables independent control of each deposition parameter at a constant value. Here we studied the deposition kinetics and narrow-gap-filling of copper thin film in supercritical carbon dioxide fluids using hexafluoroacetylacetonatecopper ($Cu(hfac)_2$) as a precursor. From the temperature dependence of the growth rate, the activation energy for Cu growth was determined at 0.45 ± 0.09 eV. The dependences of the growth rate on the H_2 and $Cu(hfac)_2$ concentrations were studied, and an apparent rate equation was obtained. The gap-filling property was found to improve as H_2 concentration increases. The crystallographic texture of the obtained film was also studied, and (1 1 1) preferential films were obtained when the H_2 concentration was high.

PACS: 81.15. −z; 82.33.De

Keywords: Supercritical carbon dioxide; Thin film deposition; Copper; Flow reactor; $Cu(hfac)_2$

1. Introduction

Thin film deposition in supercritical carbon dioxide ($scCO_2$) has attracted much interest, especially in view of applications involving microelectronics [1–3]. In this technique, organometallic compound, hereafter called a precursor, is dissolved and decomposed in $scCO_2$ fluid, usually together with a gaseous reagent [4,5]. One of the primary technological targets for this deposition technique is in applying it to the fabrication of Cu interconnects of ultra-large-scaled integrated circuits (ULSIs) as a replacement of current deposition technologies such as chemical vapor deposition and electrochemical deposition. Copper has been introduced for use in advanced ULSIs because of, for instance, its lower bulk resistivity than that of conventional Al (1.55 μΩ versus 2.50 μΩ for Al) [6], and its excellent performance against electro/stress migration [7]. In the present technology vehicle, Cu is first filled into the pre-engraved trenches and via holes using electrochemical deposition, following Cu sputtering for the conductive underlayer formation. The excess Cu is then removed by polishing the surface (chemical mechanical polishing). For this reason, metal filling of small features in addition to conformal deposition onto a convexo-concave topography have always been of serious concern in ULSI interconnect fabrication. Expected results in differentiation to existing deposition techniques include (1) very good gap-filling/conformal deposition capability in features as small as those on a deca-nanometer scale because of good diffusivity and zero surface tension of $scCO_2$ fluids, (2) good film quality due to the dissolution of reaction byproducts to $scCO_2$ fluids, (3) good thermal stability of deposited films as a result of moderate process temperatures of 150–300 °C, (4) deposition temperature is lower than chemical vapor deposition due to the solvent capability of $scCO_2$, and finally (5) potential recyclability of $scCO_2$ and unreacted precursors, which can make this process affordable and environmentally friendly.

One basic reaction arrangement for thin film deposition from $scCO_2$ is a so-called *batch* or *static* system [1,2]. In this system, the substrate and precursor are enclosed in a pressure-resistant reactor. The reactor is then filled with a gaseous reagent—we use H_2 for Cu deposition—at typically 0.1–1 MPa. Following the gas-charge, liquid CO_2 is admitted into the reactor with a high-pressure pump, and the reactor is heated so as to deposit a thin film. The temperature and pressure are controlled at

* Corresponding author. Tel.: +81 55 220 8778.
E-mail address: kondoh@ccn.yamanashi.ac.jp (E. Kondoh).
[1] Graduate student, now with Rohm Co., Ltd.

0896-8446/$ – see front matter © 2007 Elsevier B.V. All rights reserved.
doi:10.1016/j.supflu.2007.12.004

constant values. This arrangement is simple and practical, however, the reactor temperature changes during a run, and therefore, even the reaction time is not uniquely determined with respect to the start and end of the deposition reaction. The other deposition parameters, such as the partial pressures (concentrations) of H_2, precursor, and byproducts in the reactor, also vary as the process proceeds. For these reasons, besides its practicality, this arrangement is not very appropriate for fundamental study of deposition characteristics.

In our previous work, we have developed an arrangement called the *semi-batch* or *semi-dynamic* system [8]. In this arrangement, only the substrate is initially placed in the reactor and the reactor is heated at a target process temperature. The precursor is enclosed in another reservoir. The reservoir is filled with H_2 then with CO_2, and the pressure and temperature are increased so as to obtain a precursor-dissolving supercritical solution. A separation valve between the reactor and reservoir is opened and the solution is pumped to the reactor. Thus the start and end timing of deposition can be precisely determined by the valve operation and the temperature can be kept constant during deposition. Using this system, we succeeded in obtaining an activation energy for Cu growth for the first time [9]. However, the drawback of using a closed-end reactor still exists, where the reaction environment changes during deposition.

In order to solve these problems, we have developed a *flow-type* or *dynamic* reactor. The flow-type reactor enables continuous feed and exhaust of the fluid to and from the reactor, keeping the deposition parameters, such as pressure and concentrations, constant and independent. In this sense, this system functions like common dry-processing tools such as dry etchers and vapor deposition equipment. In this article, we report the development of our flow reaction system and Cu deposition characteristics from $scCO_2$ with respect to deposition kinetics and narrow-gap-filling capability.

2. Flow-type reaction system

2.1. System diagram and basic arrangement

A schematic diagram of the flow-type reaction system is shown in Fig. 1. CO_2 was supplied from a siphon cylinder into a cooling unit. Liquid CO_2 was then pressurized with a high pressure pump (JASCO PU-2086) to above the critical pressure of 7.4 MPa and was subsequently supplied to a H_2 mixing unit. The H_2 mixing unit was connected to a H_2 gas line with a pressure of 0.3–1 MPa, which enabled the flow of low-pressure gas into the high pressure fluid continuously. This mixing unit—consisting of a 6-port rotary valve, a loop pipe, and switching valves—functions like a gas injector for chromatography with an additional non-mechanical mixing unit and a damper [10]. The controllability of the H_2 content is described afterwards. The fluid—a mixture of CO_2 and H_2—was then admitted into a precursor reservoir in which the organometallic copper is placed and dissolved. The precursor-dissolving fluid was supplied to a reactor, placed horizontally in a cylindrical heater (heating-mantle), via an optical cell for *in situ* measurement of the precursor concentration. A back pressure regulator (JASCO SCF-Bpg/M) was equipped downstream of the reactor. The fluid was depressurized at the outlet of the regulator, where the unreacted precursor was collected. All the fluid components were made of 304 or 316 stainless-steel. The H_2 mixer, reservoir, optical cell and the reactor with heating mantle were placed in a thermostatic oven maintained at 40 °C in order to maintain the supercritical condition. The fluid pressure was measured with a built-in pressure gauge. The hot-wall reactor was cylindrical and made of stainless-steel, approximately 10 mm in inner diameter and 60–70 mm in length. The temperature of the reactor was measured and controlled with a thermocouple which was inserted in a small hole in the wall at one end of the reactor. During some runs, the fluid temperature was directly measured and was compared with the readout of the control thermocouple. The fluid-measuring thermocouple tip was aligned on the central axis of the reactor, and the fluid conditions were adjusted the same way as was done in the deposition experiments. The fluid temperature at the longitudinal center differed by less than 2 °C from the controlling temperature. The longitudinal distribution of the fluid temperature along the reactor length was within ±5 °C for ±25 mm and less than ±2 °C for ±10 mm.

2.2. Measurement and control of the concentrations of Cu precursor and H_2

The Cu precursor used in the present study was hexafluoroacetylacetnatecopper ($Cu(C_5HF_6O_2)_2$, abbr. $Cu(hfac)_2$). $Cu(hfac)_2$ is a dark green solid and is known to be very soluble in $scCO_2$ as well as in common solvents such as alcohol and ketones [11,12]. The concentration of the precursor was monitored with the in-line monitoring system. An optical cell having two sapphire windows for absorption measurement was installed between the precursor reservoir and the reactor (see Fig. 1). The light emitted from a halogen lamp was shone through one window by way of an optical fibre guide, and the transmitted light was collected at the other window. The collected light was guided by an optical fibre to a multichannel photodiode-array spectrometer.

The calibration line for the absorbance measurements was obtained preliminarily. Weighed $Cu(hfac)_2$ was placed within the optical cell, and all connection ports were plugged with blind plugs except the CO_2 inlet. The optical cell was placed in a thermostatic oven maintained at 40 °C. After pressurization the inlet valve was closed and the chamber was stirred with a magnetic stirrer. Visible spectra were then taken with the above-mentioned spectrometer for different amounts of $Cu(hfac)_2$. Fig. 2 shows spectra of $Cu(hfac)_2$ taken at 8 MPa and 40 °C. The absorbance spectra peak at around 700 nm and has a valley at around 500 nm, indicating that the solution is green. These profiles agree well with the data in literature [13]. The absorbance increased linearly at 700 nm with increasing the concentration of $Cu(hfac)_2$; from this fact, we obtained the calibration curve line at the wavelength of 700 nm. From the slope of the calibration line, the molar absorbancy was determined at 35.8 mol l^{-1} cm^{-1} at 40 °C and 8 MPa. In deposition experiments, we kept the concentration of $Cu(hfac)_2$ constant

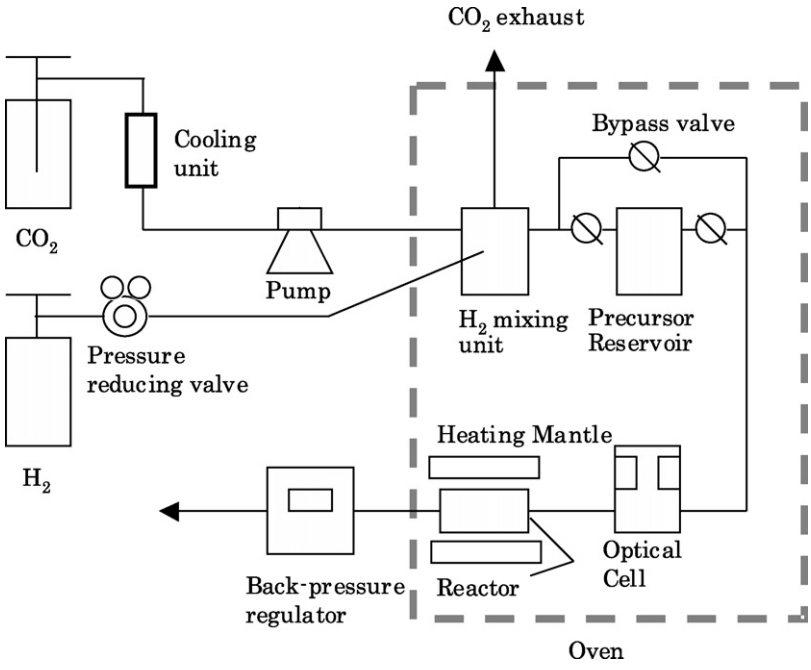

Fig. 1. Schematic diagram of the flow-type reaction system developed.

controlling the bypass-valve (Fig. 1), in order to dilute the high-concentration outflow from the reservoir, bypassing pure $scCO_2$. The valve operation was carried out intermittently by monitoring the $Cu(hfac)_2$ concentration. The maximum concentration in this work was approximately 380 ppm (parts ber million). Fig. 3 exhibits time change of $Cu(hfac)_2$ concentration measured during a deposition run for 20 min. The valves of the reservoir were opened and closed at the times indicated by the arrows. The $Cu(hfac)_2$ concentration became stationary at approximately 200 s after each valve operation. This time is short enough compared to the nominal deposition time, 20 min in this case. The average $Cu(hfac)_2$ concentration was calculated for the time span where the concentration exceeded 2% of the maximum value, and was used as a representative concentration value. As described later, the growth rate was found zero-order against $Cu(hfac)_2$ concentration. Therefore, concentration change during a deposition run does not affect the kinetic analysis of film growth.

The concentration of H_2 was adjusted by changing its supply pressure in the H_2 mixing unit. The concentration was measured with a gas-chromatograph by sampling the vaporized fluid at the outlet of the apparatus. The relationship between the supply pressure and the H_2 concentration exhibited very good controllability (Fig. 4). In contrary to the precursor concentration dependence, the deposition process was found to be sensitive to the concentration of H_2 (discussed later); therefore, the degree of accuracy in the H_2 concentration is really crucial for styding deposition kinetics. Finally it was noted that the highest

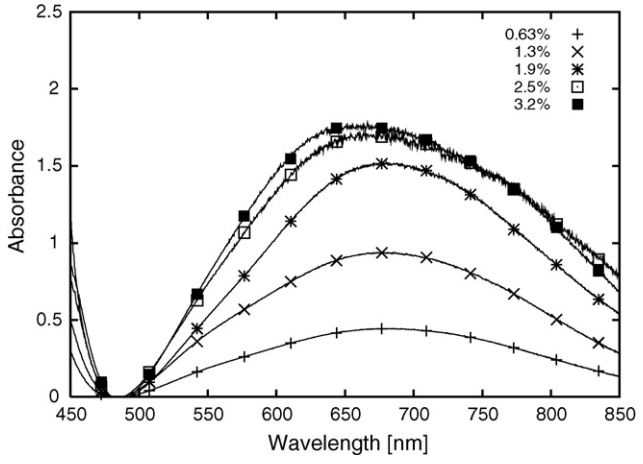

Fig. 2. Visible absorbance spectra of $Cu(hfac)_2$ dissolved in $scCO_2$ taken at a pressure of 8 MPa and a temperature of 40 °C.

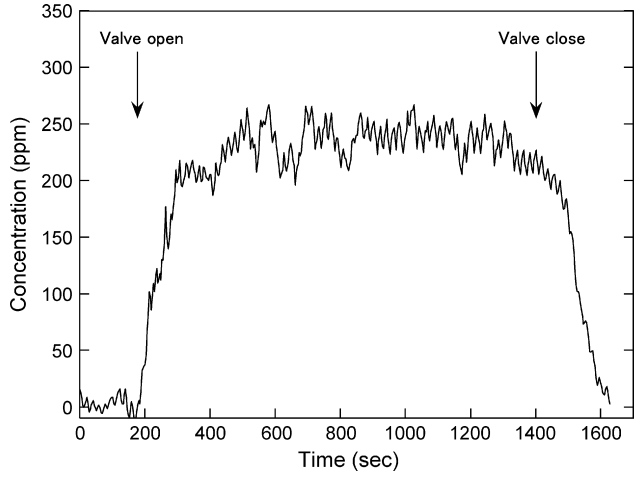

Fig. 3. Typical time change of $Cu(hfac)_2$ concentration during a deposition run. The arrows indicate the times when values were operated to supply $Cu(hfac)_2$.

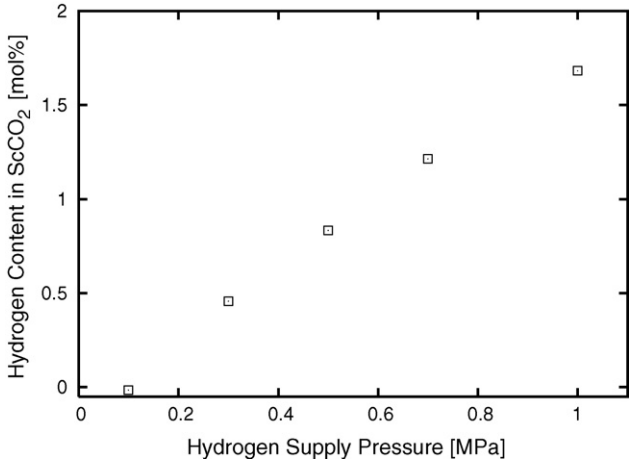

Fig. 4. H_2 concentration in $scCO_2$ as a function of H_2 supply pressure.

H_2 concentration obtained from this study was 1.8%, which is still 1/5 to 1/10 of that from our past batch-reactor experiments [8].

3. Conditions of deposition experiments

Deposition experiments were carried out using the apparatus described in the previous section. $Cu(hfac)_2$ was purchased from Tri-Chemical Laboratories Inc. (Yamanashi, Japan). The substrates used were TiN-coated Si wafer pieces having test patterns for gap-fill assessment. We used the same set of wafers in our past experiments [8].

After placing a piece of wafer (ca. 10×50 mm) faceup and horizontally in the middle of the reactor, the reactor was closed and the residual gas in the system was purged with gaseous CO_2. The outlet valve of the reservoir and the bypass valve were closed together, and the H_2-added $scCO_2$ fluid was pumped into the precursor reservoir at operation pressure. The inlet and outlet valves of the reservoir were then closed, and the fluid was introduced into the reactor through the bypass valve. The deposition was then started by switching the flow of $scCO_2$ from the bypass line to the reservoir line, and the elapsed time was recorded.

The deposition conditions are summarized in Table 1. After deposition, cross-sections of the specimens were observed with a JOEL JSM6500F field-emission secondary electron microscope (SEM), the film thicknesses were measured with a surface profilometer (DekTak^{TM}), and θ–2θ X-ray diffraction measurements were performed with a Rigaku RAD1 X-ray diffractometer using Cu K_α emission line.

Table 1
Deposition conditions of this work

Temperature	180–320 °C
Pressure	8 MPa
Hydrogen concentration	0.4–1.8%
$Cu(hfac)_2$ concentration	15–380 ppm
Deposition time	20–60 min

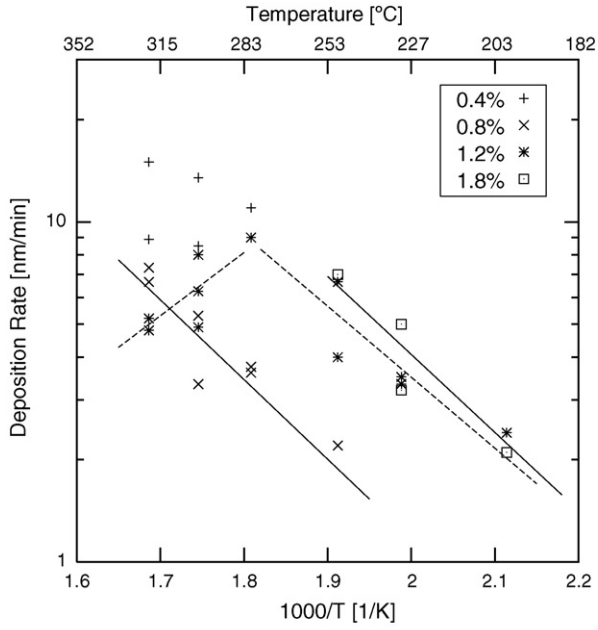

Fig. 5. Arrhenius plots of deposition rate for different H_2 content.

4. Results and discussion

4.1. Deposition kinetics

4.1.1. Temperature dependence

Activation energy for the growth: Fig. 5 shows Arrhenius plots of the deposition rate obtained for different hydrogen concentrations. A linear relationship with negative slope is observed for each hydrogen content. Table 2 lists the activation energies determined from the data sets shown in Fig. 5. The data set for 0.4 mol% H_2 is not very reliable, because the deposits obtained were porous or granular. Practically no deposition occurred at temperatures lower than those listed in Table 2. In other words, film growth did not start even at higher temperatures ($\gtrsim$ 250 °C) when H_2 concentration was not sufficiently high ($\gtrsim$ 0.5%). This behavior is discussed later. By assuming that all the positive activation energy values for 0.8, 1.2, and 1.5% belong to the same population, we obtained the activation energy for Cu growth of 0.45 ± 0.09 eV. This value was in very good agreement with our previously reported value of 0.42 ± 0.12 eV for the same $Cu(hfac)_2$–H_2 chemistry but using a batch-type reactor [8]. The observed value of 0.45 eV is lower than the ones reported in thermal chemical vapor deposition [14,15], but is similar to the results of plasma chemical vapor deposition [16]. This is likely due to the solvation effect of $scCO_2$[2,8], as well as the

Table 2
Activation energies for Cu deposition

H_2 concentration (%)	Activation energy (eV)	Temperature range (°C)
0.8	0.47 ± 0.08	250–320
1.2	0.41 ± 0.08	200–280
	-0.37 ± 0.27	280–320
1.5	0.46 ± 0.13	200–250

active role of the solvent $scCO_2$ in removing reaction byproducts [17,18]. In a similar report on chemical vapor deposition for Cu thin film growth from dipivaloylmethanecopper ($Cu(dpm)_2$, $Cu(tmod)_2$) using a batch $scCO_2$ system, the activation energy, 0.54 eV, was lower than in chemical vapor deposition [18]. From these it is suggested that a common deposition mechanism functions for Cu growth from Cu(II) β-diketonates. On the other hand, the activation energies for the thermal decomposition of $Cu(hfac)_2$ and acetylacetonatecopper ($Cu(acac)_2$) were reported to be 0.86 [19] and 0.65 eV [20], respectively, 1.5–2 times higher than our values. However, it should be noted that these values were obtained for thermal decomposition without a reduction agent nor catalytic substrate. In thin film deposition, a growing surface plays a catalytic role and thus decreases the activation energy for reaction. In this sense, deviation from our value is quite reasonable.

Growth rate reduction at higher temperatures: When the temperature was high, we obtained the negative temperature dependence of the growth rate. The activation energy for the H_2 concentration of 1.2% was -0.37 ± 0.27 eV. We observed similar behavior in our previous study on Cu deposition [2] and Ru deposition [21] with a batch reactor, which may suggest the generality of this phenomenon. The reason for this phenomenon is not clear at present. The decrease in thickness at higher temperatures is not always observed in chemical vapor deposition. In typical vapor deposition chemistry, the deposition rate levels off at higher temperatures when the rate-determining step of growth changes from the reaction-limited to the transport-limited of reaction species.

The negative temperature dependence can appear when a reverse reaction becomes significant with increasing temperature. Possible reverse reactions are the desorption of adsorbing species or an etching reaction. As discussed later, hydrogen and $Cu(hfac)_2$ are thought to be adsorbed to the surface. Hydrogen chemisorbs very strongly to metal surfaces, and therefore hydrogen desorption does not proceed favorably. The desorption of the adsorbing $Cu(hfac)_2$ or its intermediate products is more likely to occur.

4.1.2. Hydrogen and precursor concentration dependences

Fig. 6 shows the dependence of the copper growth rate on the H_2 concentration obtained at 250 °C. The growth rate increased with H_2 concentration and leveled off above around 1 %. As stated before, no growth was observed when the H_2 content was 0.4 %.

The fitting curve in Fig. 6 was obtained using the following equation based on a Langmuir-type adsorption isotherm,

$$\text{Deposition rate} \propto \frac{(KX_{H_2})^n}{1+(KX_{H_2})^n} \quad (1)$$

where X_i is the concentration of species i in the ambient, and K and n are the fitting parameters, hereafter. The extrapolated straight line intersects the horizontal axis at about 0.6%.

The dependence of the growth rate on the concentration of $Cu(hfac)_2$ was also studied. We did not observe clear dependence on the $Cu(hfac)_2$ concentration. This suggests that the growth rate is zero-order with respect to the $Cu(hfac)_2$ concentration.

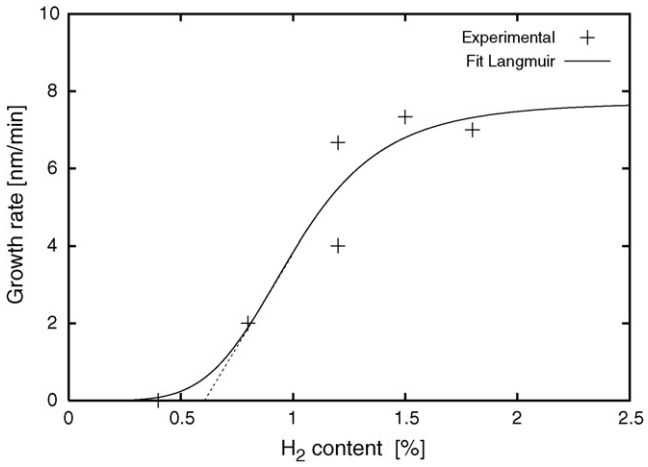

Fig. 6. Dependence of growth rate on the H_2 concentration. The deposition temperature and pressuer were 250 °C and 8 MPa, respectively.

From these results, we obtained an apparent overall rate equation,

$$\text{Deposition rate} \propto \frac{(KX_{H_2})^n}{1+(KX_{H_2})^n} X^0_{Cu(hfac)_2} \exp\left(-\frac{5200}{T}\right). \quad (2)$$

4.1.3. Surface reaction mechanisms

Two basic surface reaction models based on the sorption isotherm are known, namely Langmuir–Hinshelwood and Rideal–Eley mechanisms. A Langmuir–Hinshelwood type reaction proceeds between the surface-adsorbed species, and a Rideal–Eley type reaction occurs between the surface-adsorbed and the gaseous species.

The rate equation of a Langmuir–Hinshelwood type reaction between surface species A and B are expressed by

$$r \propto \theta_A \theta_B, \quad (3)$$

where θ_i is the surface coverage of species i. A Rideal–Eley type reaction has a different formula

$$r \propto \theta_A p_B, \quad (4)$$

assuming species A is surface-adsorbed and species B is incident to the surface from the environment.

In the previous subsection, we concluded that the Langmuir-type adsorption of hydrogen dominates the overall reaction process, where the growth rate increases with the concentration of H_2 but saturates at higher H_2 concentrations. By following Eq. (3) we can write the formula, $\theta_H \propto (KX_{H_2})^n/[1+(KX_{H_2})^n]$. This obviously tells us that the adsorbed hydrogen is involved in the growth reaction. Conversely, we found no $Cu(hfac)_2$ concentration dependence of the growth rate. This means that reaction (4) does not hold and that the surface is almost saturated with $Cu(hfac)_2$ (or presumably its intermediate products), i.e., $\theta_{Cu(hfac)_2} \approx 1$.

Such high coverage occurs when $Cu(hfac)_2$ is adsorbed well. $Cu(hfac)_2$ is a polar molecule and has a strong intermolecular interaction, as can be understood from its high melting point of about 98 °C [22]. Obviously $Cu(hfac)_2$ has a large heat of adsorption and is thought to adhere easily to the sur-

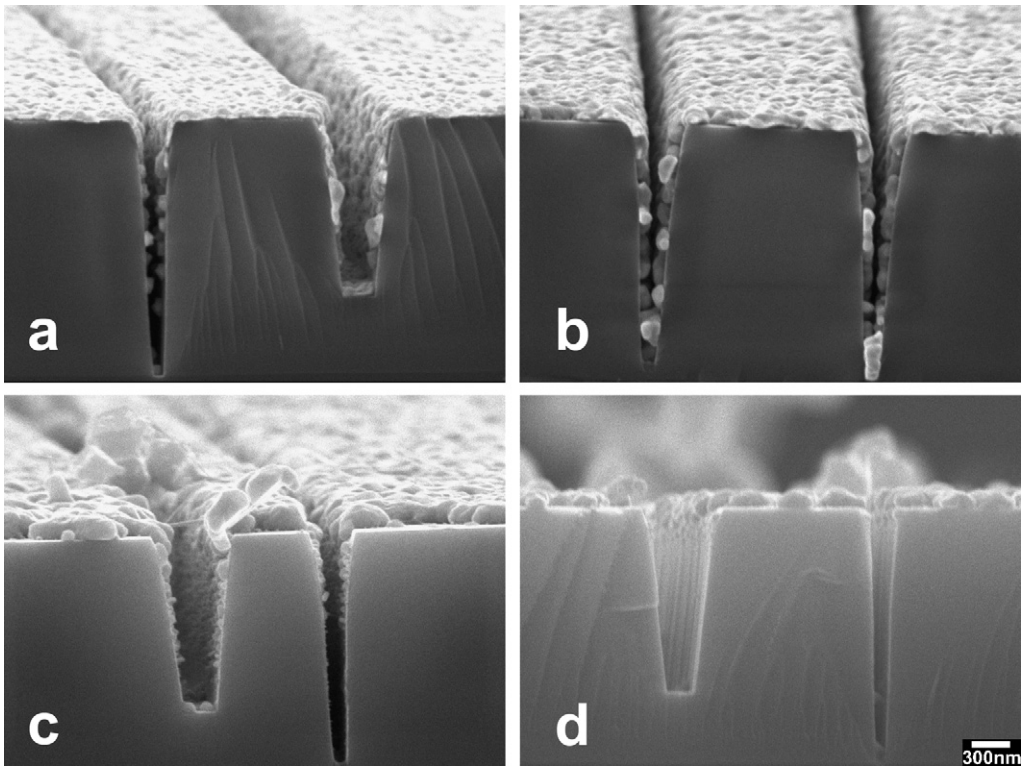

Fig. 7. Cross-sectional SEM photos of Cu filled in small trenches at (a) 230 °C, (b) 250 °C, (c) 300 °C, and (d) 320 °C. The H_2 concentration was fixed at 1.2%. The scale bar is 300 nm.

face. A very high molecular number density of $Cu(hfac)_2$ in $scCO_2$ may enable the adsorption to occur more easily compared to gas-phase reactions. Therefore, the coverage of $Cu(hfac)_2$ should be much higher than that of dissociated H atoms.

We now conclude that the Cu growth proceeds via the Langmuir–Hinshelwood mechanism, for instance,

$$H_2^{sc} \rightarrow 2H^{ad} \quad \text{(R1)}$$

$$Cu(hfac)_2^{sc} \rightarrow Cu(hfac)_2^{ad} \quad \text{(R2)}$$

$$2H^{ad} + Cu(hfac)_2^{ad} \rightarrow Cu + 2Hhfac^{ad} \quad \text{(R3)}$$

$$Hhfac^{ad} \rightarrow Hhfac^{sc}, \quad \text{(R4)}$$

where subscripts sc and ad indicate 'in $scCO_2$' and 'adsorbed', respectively. In our case, the rate-determining step is likely to be involved in reaction (R3). The solvent capability naturally functions better in this reaction, which agrees fairly well with our observation. An overall activation energy of surface reactions is potentially dependent on the coverage of the adsorbed species. When the coverage θ is large the activation energy becomes close to that of the rate-determining step, whereas when $\theta \ll 1$ it approaches the value of a heat of adsorption. We did not observe the dependence of the activation energy on hydrogen concentration in the extent of our experiments. The reason for this is probably due to over simplification of the reaction mechanism. Our adsorption isotherm (Eq. (1)) actually assumes a high-order adsorption 'reaction'. The n value obtained from the curve fitting was 5.0, and thus the equation is very sensitive to the H_2 concentration. This is seen as a quick decay of the filling curve in Fig. 4 as X_{H_2} approaches 0, and a quick saturation at around $X_{H_2} = 1.2$. (The first-order Langmuir equilibrium isotherm, $n = 1$ in Eq. (1), shows more gradual saturation.) A reaction model which requires the successive addition of hydrogen can be proposed for explaining this apparent high-order reaction. The presence of parallel reactions that proceed competitively with the Cu deposition reaction can also give an apparently high reaction order. In this case, θ_H can have a higher order factor like $\theta_H^a (a > 1)$, which produces a similar mathematical results as Eq. (1) but with a smaller n value. Formation of oxide from impurity H_2O in CO_2 and its reduction by H can be listed as possible parallel reactions that compete with the deposition reaction.

4.2. Surface morphology and gap-filling capability

Fig. 7 shows cross-sectional SEM photos of Cu filled in small trenches for different deposition temperatures. The H_2 concentration was fixed at 1.2%.

The film deposited at 230 °C (Fig. 7(a)) shows a flat topography. Good conformability is observed even inside the trench 500 nm-in-width at the opening (right side of the photo). In contrast, the deposit is granular in the 300 nm-wide trench (on the left). The deposit becomes more discontinuous in a deeper part, and no deposit was observed neat the bottom.

When the temperature was increased to 250 °C (Fig. 7(b)), a more conformal film was observed in these 300 nm-wide trenches. The surface is flatter and the film is thicker. The films in the trenches are slightly more granular than that of the top, suggesting that poorer nucleation occurred. At 280 °C (photo not shown), the film's thickness increased. The deposition inside the trench was as good as 250 °C.

The surface of the film obtained at 300 °C (Fig. 7(c)) is rougher and agglomerated. A thinner film is formed at the sidewall and bottom of the trenches. This tendency becomes clearer at 300 °C (Fig. 7(d)) exhibiting a much smaller film thickness. At this temperature, hillocks or whiskers were observed on the film surface.

Fig. 8 shows cross-sectional SEM photos of Cu filled in small trenches for different H_2 concentrations at a deposition temperature of 250 °C. It is clearly observed that the surface roughness, grain continuity, and gap-fill property improve with H_2 content.

As we have seen so far, the filling capability was found to be highly dependent on the H_2 concentration and the deposition temperature. Too high a temperature resulted in the formation of granular deposits and even abnormal growth, and too low a temperature or less H_2 concentration resulted in poor nucleation. A higher H_2 concentration was favorable to ignite the prompt nucleation and thus to form a thin continuous film.

Thin film deposition inside a longitudinal feature can be analyzed by using a Thiele diffusion model [23]. The Thiele model deals with the balance between the amounts of incoming and consumed species inside the feature. This model has been successfully employed in analyzing the step coverage in chemical vapor deposition [24] and was applied to the conformability analysis in thin film deposition from $scCO_2$[25].

Now let us assume that a sufficient amount of chemical species is supplied deep inside the feature. Obviously, we can expect better conformal deposition to take place. Conversely, if the consumption of the species is large, the conformability will become poor. As discussed above, the growth rate is, in our case, dominated by the H_2 concentration. For simplicity, we first discuss three extreme cases of the H_2 concentration. When the H_2 concentration is lower than approximately 0.5%, no film growth occurs. As a result, the H_2 concentration in a trench becomes uniform; however, this situation is not of concern. As the concentration of the supplied H_2 increases, the Cu growth rate increases and the H_2 concentration deep in the trench will decrease. When the concentration of the supplied H_2 is high enough, the growth rate becomes independent of the H_2 concentration (see Fig. 6); and therefore, the distribution of H_2 in the trench becomes uniform, which results in good step coverage. From this discussion, the most critical condition with respect to the deposition conformability is when the H_2 concentration is about 1.2% at which the growth rate starts to level off.

From simple calculations, we found that there is no expected H_2 concentration decrease along the trench depth even under the above-mentioned extreme condition (see Appendix A). This consequence is in fact obvious, because only very small amount of H_2 is consumed for the Cu growth. However, indeed, we have observed the improvement of film conformability as the H_2 concentration increased. The reason for this discrepancy is not clear at present. The diffusion of other species such as $Cu(hfac)_2$ can be a reason, whereas the diffusion coefficient in $scCO_2$ cannot be too small to give a large inhomogeneity in the concentration. Presumably the nucleation behavior is more dominating. The nucleation is a more complex phenomenon than the continuous film growth and may have different kinetics. Once Cu

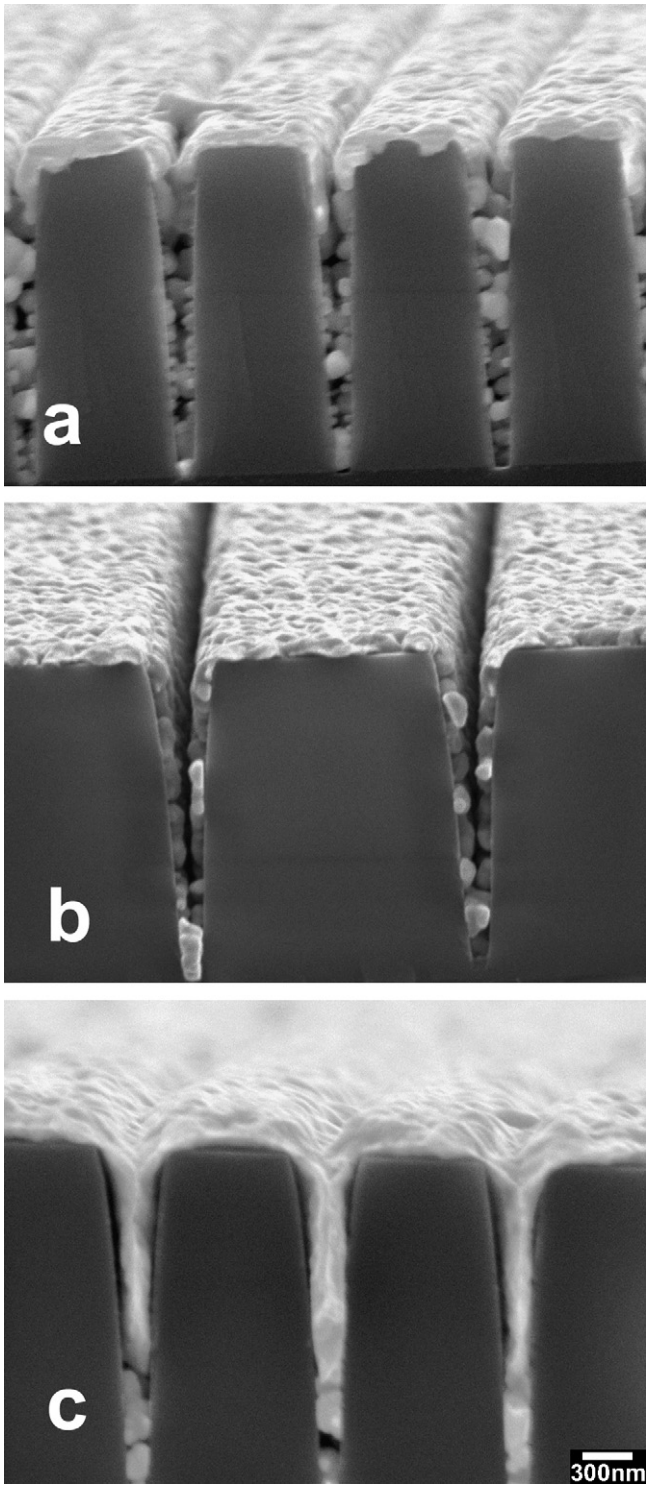

Fig. 8. Cross-sectional SEM photos of Cu filled in small trenches at a H_2 concentration of (a) 1.0%, (b) 1.2%, and (c) 1.5%. The deposition temperature was fixed at 250 °C. The scale bar is 300 nm.

Table 3
X-ray θ–2θ diffraction (1 1 1)/(2 0 0) intensity ratio

H_2 conc. (%)	Temp. (°C)	(1 1 1)/(2 0 0) Ratio
0.4	280	4.2
0.8	280	5.3
1.2	280	6.7
1.2	300	5.6
1.2	320	4.2
(Powder)	–	2.17

growth starts somewhere inhomogeneously, the growth proceeds preferably thereon, which accelerates the inhomogeneity.

4.3. Film texture

Finally the results of the film texture analysis with θ–2θ X-ray diffractometry are shown in Table 3. The film texture is technologically important, because the reliability of ULSI interconnect improves as the ratio of the (1 1 1)-plane intensity to the (2 0 0) intensity increases [26]. The (1 1 1)/(2 0 0) intensity ratio was higher than the one listed in the database of the Joint Committee for Powder Diffraction Studies (JCPDS), indicating preferential growth of (1 1 1) planes parallel to the substrate. The (1 1 1)/(2 0 0) intensity ratio increased slightly with increasing the H_2 concentration but decreased with deposition temperature.

It is well known that (1 1 1) planes of face-centered-cubic (fcc) metals tend to develop during thickening of thin film. This is because fcc (1 1 1)—Cu has an fcc structure—is the lowest-energy plane and therefore grain boundaries sweep the surface so as to minimize the total surface energy. By comparing the data of Table 3 with Fig. 5, it seems that the (1 1 1)-texture developed as the growth rate increased. In our experiments the deposition times were fixed, meaning that the (1 1 1)-textured films have a greater thickness. This is consistent with the above discussion.

Another possible reason for the (1 1 1)-texturing is the attractive interaction between Cu and substrate. Stronger interaction decreases the interfacial energy, which leads to the formation of two-dimensional nucleation [27]. According to classical nucleation theory, prompt nucleation occurs when the interfacial energy is low and/or when the growth rate is high. Our observations corroborate those of this discussion.

5. Conclusions

Cu thin film growth from $scCO_2$ using $Cu(hfac)_2$ as a precursor was described with respect to growth kinetics and narrow-gap-filling. We used H_2 gas as a reducing agent. A newly developed flow reaction system was employed in this study. This system was designed to enable continuous addition of low-pressure H_2 gas to the high pressure $scCO_2$ fluid, maintaining the deposition parameters constantly and independently. The molar H_2 and $Cu(hfac)_2$ concentrations, and temperature were varied in the ranges of 0.4–1.8%, 15–380 ppm and 180–320 °C, respectively. The pressure was fixed at 8 MPa. We obtained the following results.

(1) The activation energy for Cu growth was determined at 0.45 ± 0.09 eV. A negative temperature dependence was observed at higher temperatures.
(2) The growth rate increased with H_2 concentration and leveled off above around 1 %. When the H_2 content was decreased to 0.4 %, the obtained films were discontinuous and rough. The film growth was found to be a zero-order reaction with respect to the $Cu(hfac)_2$ concentration. An apparent overall rate equation was obtained. The reaction of the film growth proceeds via the Langmuir–Hinshelwood mechanism.
(3) There is a moderate temperature that is appropriate for good film conformability. Increasing the H_2 concentration resulted in better gap-filling performance.
(4) The obtained films were (1 1 1)-textured. The (1 1 1)-texturing improved with increasing the H_2 concentration but decreased with deposition temperature.

Acknowledgements

Part of this work was supported by a Grant-in-Aid for Scientific Research from the Japan Society for the Promotion of Science and by the Semiconductor Technology Academic Research Center (STARC). We greatfully acknowledge with useful discussion with the STARC project members, H. Tanaka, M. Sato, H. Yano, Y. Shimogaki, M. Sugiyama, and M. Yoshimaru.

Appendix A. Distribution of a chemical species in a longitudinal slit

Uniformity of the film thickness in a longitudinal thin chamber is determined by the balance between the diffusion transport and the consumption of the growth-contributing species as long as advection/convection is insignificant.

Let us consider a two-dimensional longitudinal slit like that shown in Fig. A.1. The species in attention diffuses along x-axis one-dimensionally from the left-side, where its concentration $C(x)$ is fixed at C_0 at $x = 0$. The species is annihilated on the slit surface at a rate of S (>0). The mass flux incoming to an infinitesimally small region dx is $J_{in} = -D\mathrm{d}C/\mathrm{d}x$, here D is the diffusion constant as usual. Likewise, the outgoing flux at $x + \mathrm{d}x$ is $J_{\mathrm{out}} = -D(\mathrm{d}C/\mathrm{d}x - \mathrm{d}^2C/\mathrm{d}x^2)$. By considering the mass balance in the control volume in an infinitesimally small

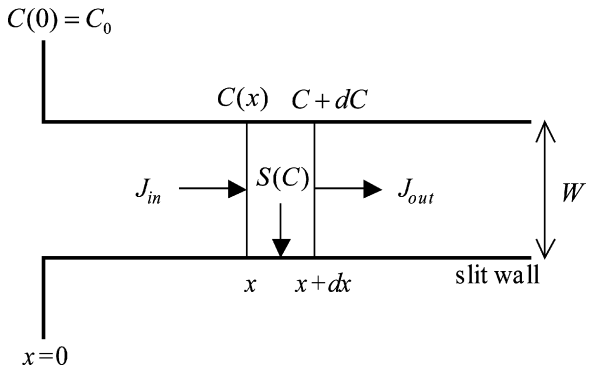

Fig. A.1. Two-dimensional longitudinal slit model.

time interval, we obtain a steady-state diffusion equation,

$$DW\frac{d^2C}{dx^2} - 2S = 0. \quad (A.1)$$

If S is constant—this is an extreme case that we discussed in the main text—a general solution for Eq. (A.1) is a simple quadratic equation. A solution that satisfies the physical requirements is a convex downward parabola that is defined between $x = 0$ and $x = L_{ex}$, where L_{ex} is the x coordinate of the vertex. As a special case of $C(L_{ex}) = 0$, the distribution of the species becomes most inhomogeneous, and then,

$$L_{ex} = \sqrt{\frac{C_0 DW}{S}}, \quad (A.2)$$

which we define here as the extinction length. When the extinction length L_{ex} is large enough compared to the depth of a trench, like that shown in Fig. 4, the distribution of the species is practically uniform.

By substituting the following experimental values to Eq. (A.2), $C_0 = 0.4$ mol/m^3, $D = 10^{-7}$ m^2/s, $W = 10^{-7}$ m, and $S \approx 2 \times 10^{-5}$ mol/m^2/s, we obtain $L_{ex} = 14\,\mu$m, which is dozens of times larger in magnitude than the actual trench depth.

References

[1] E. Kondoh, H. Kato, Characteristics of copper deposition in a supercritical CO_2 fluid, Microelectron. Eng. 64 (2002) 495–499.

[2] E. Kondoh, Deposition of Cu and Ru thin films in deep nanotrenches/holes using supercritical carbon dioxide, Jpn. J. Appl. Phys. 43 (2004) 3928–3933.

[3] J.M. Blackburn, D.P. Long, A. Cabañas, J.J. Watkins, Deposition of conformal copper and nickel films from supercritical carbon dioxide, Science 294 (2001) 141–145.

[4] B.M. Hybertson, B.N. Hansen, R.M. Barkley, R.E. Sievers, Deposition of palladium films by a novel supercritical fluid transport chemical deposition process, Mater. Res. Bull. 26 (1991) 1127–1133.

[5] O.A. Louchev, V.K. Popov, E.N. Antonov, The morphological stability in supercritical fluid chemical deposition of films near the critical point, J. Cryst. Growth 155 (1995) 276–285.

[6] Y.D. Chen, A. Reisman, I. Turlik, D. Temple (Eds.), CRC Handbook of Electrical Resistivities of Binary Metallic Alloys, CRC Press, 1983.

[7] J. Li, T.E. Seidel, J.W. Mayer, Copper-based metallization in ULSI structures, MRS Bull. 19 (1994) 15–18.

[8] E. Kondoh, K. Shigama, Deposition of Cu thin films from supercritical carbon dioxide using hexafluoroacetylacetnatecopper, Thin Solid Films 491 (2005) 228–234.

[9] E. Kondoh, K. Shigama, Nanoscale deposition in supercritical fluids: Cu metallization process and barrier metal deposition possibility, in: Proc. Advanced Metallization Conf. 2003, Material Research Society, PA, 2004, pp. 583–588.

[10] Japanese published unexamined patent application 2004–249487 (2004).

[11] N.S. Borgharkar, G.L. Griffin, H. Fan, A.W. Maverick, Solution delivery of Cu(hfac)$_2$ for alcohol-assisted chemical vapor deposition of copper, J. Electrochem. Soc. 146 (1999) 1041–1045.

[12] A.F. Lagalante, B.N. Hansen, T.J. Bruno, R.E. Sievers, Solubilities of copper(II) and chromium(III) β-diketonates in supercritical carbon dioxide, Inorg. Chem. (1995) 5781–5785.

[13] Y. Inada, T. Horita, Y. Yokooka, S. Funahashi, Kinetic effect of cosolvents on the metalation reaction of porphyrin with bis(β-diketonato)copper(II) in supercritical carbon dioxide, J. Supercrit. Fluids 31 (2004) 175–183.

[14] D.-H. Kim, R.H. Wentorf, W.N. Gill, Low pressure chemically vapor deposited copper films for advanced device metallization, J. Electrochem. Soc. 140 (1993) 3267–3279.

[15] Y.D. Chen, A. Reisman, I. Turlik, D. Temple, Cu CVD from copper(II) hexafluoroacetylacetonate. I. A cold wall reactor design, blanket growth rate, and natural selectivity, J. Electrochem. Soc. 142 (1995) 3903–3911.

[16] N. Awaya, K. Ohno, Y. Arita, The effect of adding hexafluoroacetylacetone on chemical vapor deposition of copper using Cu(I) and Cu(II) precursor systems, J. Electrochem. Soc. 142 (1995) 3173–3179.

[17] E. Kondoh, Copper deposition characteristics from a supercritical CO_2 fluid, in: Proc. Advanced Metallization Conf. 2002, Material Research Society, PA, 2003, pp. 463–468.

[18] Y. Zong, J.J. Watkins, Kinetics of Cu deposition by the hydrogen reduction of $Cu^{(II)}(tmod)_2$ in supercritical CO_2, in: Proc. Advanced Metallization Conf. 2004, Material Research Society, PA, 2005, pp. 353–357.

[19] R. Garriga, V. Pessey, F. Weill, B. Chevalier, J. Etourneau, F. Cansell, Kinetic study of chemical transformation in supercritical media of bis(hexafluoroacetylacetonate)copper(II) hydrate, J. Supercrit. Fluids 20 (2001) 55–63.

[20] S. Yoda, Y. Takebayashi, T. Furuya, K. Otake, Decomposition of metal acetylacetonate in supercritical carbon dioxide, PB-2–29, in: Proceedings of 8th International Symposium on Supercritical Fluids, 2006.

[21] E. Kondoh, Deposition of Ru thin films from supercritical carbon dioxide fluids, Jpn. J. Appl. Phys. 44 (2005) 5799–5802.

[22] Date sheet from the material supplier.

[23] O. Levenspiel, Chemical Reaction Engineering, second ed., John Wiley & Sons, New York, 1972, Ch. 14.

[24] T. Sorita, S. Shiga, K. Ikuta, Y. Egashira, H. Komiyama, The formation mechanism and step coverage quality of tetraethylorthosilicate-SiO_2 films studied by the micro/macrocavity method, J. Electrochem. Soc. 140 (1993) 2952–2959.

[25] F. Kano, H. Uchida, K. Yui, S. Koda, Step coverage of titanium oxide thin films deposited on trench structures in supercritical carbon dioxde, PB-2–28, in: Proceedings of 8th International Symposium on Supercritical Fluids, 2006.

[26] Q.-T. Jiang, M.E. Thomas, Recrystallization effects in Cu electrodeposits used in fine line damascene structures, J. Vac. Sci. Technol. B 19 (2001) 762–766.

[27] E. Kondoh, Material characterization of Cu(Ti)-polyimide thin film stacks, Thin Solid Films 359 (2000) 255–260.